

Adsorption kinetics and thermodynamics and equilibrium of ibuprofen from aqueous solutions by activated carbon prepared from *Lemna minor*

Davoud Balarak^a, Zeynab Taheri^b, Moo Joon Shim^c, Seung-Mok Lee^{c,*}, Choong Jeon^{d,*}

^aDepartment of Environmental Health, Health Promotion Research Center, Zahedan University of Medical Sciences, Zahedan, Iran, email: dbalarak2@gmail.com

^bStudent Research Committee, Zahedan University of Medical Sciences, Zahedan, Iran, email: mbehdasht75@gmail.com

^cDepartment of Environmental Engineering, Catholic Kwandong University, Gangneung 25601, South Korea, Tel. +82-33-649-7535; emails: leesm@cku.ac.kr (S.-M. Lee), moojoonshim@gmail.com (M.J. Shim)

^dDepartment of Biochemical Engineering, Gangneung-Wonju National University, Gangneung 25457, South Korea, Tel. +82-33-640-2405; email: metaljeon@gwnu.ac.kr

Received 24 July 2020; Accepted 30 November 2020

ABSTRACT

In this study, the adsorption of Ibuprofen (IPF) antibiotics from aqueous solutions by *Lemna minor* activated carbon (LMAC) was studied in a batch adsorption system. LMAC exhibited a large surface area of 1,164.5 m²/g, the total pore volume of 0.417 cm³/g, yield of 0.482, and pH_{pzc} of LMAC were 6.6. In addition, adsorption was endothermic and spontaneous and was highly pH-dependant, the optimum pH was 3. The equilibrium data obtained were analyzed by Langmuir, Freundlich, Temkin, and Dubinin–Radushkevich isotherm models. The equilibrium time was found to be 75 min. The Langmuir model gave the best correlation with the experimental data. Maximum adsorption capacities of IPF were 124.5, 141.8, 159.2, and 181.2 mg/g at 283, 298, 313, and 328 K, respectively, and their adsorption mechanism was the monolayer adsorption on the surface of LMAC. The adsorption was found to follow the pseudo-second-order kinetics. Both film diffusion and intra-particle diffusion were found to be the major process facilitated the adsorption. The optimum conditions for IPF adsorption were at IPF concentration of 25 mg/L, pH of 3, LMAC dose of 1.2 g/L, the contact time of 75 min, and temperature 328 K. The best efficiency for the removal of IPF was obtained 99.98%.

Keywords: Activated carbon; Ibuprofen; Isotherm; *Lemna minor*; Thermodynamics

1. Introduction

In the past few decades, the presence of antibiotic compounds has been detected at trace concentrations (ng/L to µg/L) in many surface waters [1,2]. The presence of these substances with complex structure can adversely affect the aqueous environment by reducing photosynthesis activity [3,4]. Moreover, most of these compounds can cause skin irritation, respiratory problems, and can also increase cancer and cell mutation risk in humans [5,6]. Therefore, effluents

containing antibiotics require efficient treatment before being discharged into the environment.

Ibuprofen (IPF) is a widely used anti-steroidal and anti-inflammatory drug for treating inflammation, pain, fever, rheumatoid arthritis, and migraines [7,8]. As the third widely consumed drug, the concentration of IPF in the effluent from the wastewater treatment plant range up to 25 mg/L [9,10]. Moreover, just as other pharmaceutical products, IPF could be leached directly or indirectly into groundwater through

* Corresponding authors.

man's daily practices [11]. The removal of IPF with conventional techniques was less efficient due to its persistent nature [12]. However, several techniques such as chemical ozonation, photocatalysis oxidation, Fenton process, sonochemical degradation, and adsorption have been explored as an alternative to conventional treatment techniques [13–15].

Among the mentioned techniques, adsorption has been considered as the most attractive technology due to its high efficiency, its simplicity, and low-cost [16,17]. It is a method that transfers pollutants from the liquid phase to a solid phase therefore reducing the bioavailability of stable and aromatic species to living organisms [18]. Adsorbents such as resins, carbon nanotubes, and magnetic nanocomposite, and nanoparticles that are commonly used for pollutant removal have some disadvantages requiring high costs associated with their subsequent treatment and regeneration [19–23].

Among all of the adsorbents, carbon is a versatile adsorbent that is heavily used in the removal of various pollutants [24].

Carbons prepared from agricultural wastes such as bamboo, *Lemna minor*, *Azolla filiculoides*, canola, peanut hull, etc., have been further developed in recent years for the adsorption of antibiotics from aqueous environments due to its abundance and cheapness [25–27].

Activation of carbon will be both physical and chemical. Physical activation is performed at higher temperatures in the presence of gases such as carbon dioxide, steam, etc. whereas chemical activation is carried out by dehydrating agents and oxidants such as HNO_3 , ZnCl_2 , etc. Chemical activation has its own advantages such as leading to a higher yield, employing lower temperature, and shorter activation time, which is preferred over physical activation (25).

The *L. minor* is one of the wide-spread aquatic plant which is belonged to duckweed species with special characteristics including rapid growth, high nutritional value, and high water purification capabilities have been used to remove the pollutant from water and wastewater [28,29]. Several studies to remove the heavy metal, dyes, antibiotics, etc., by the *L. minor* have been conducted by the scientists [30,31]. Activated carbon (AC) has a high surface area which results from its porous surface structure [32,33]. There have been proposals to develop new adsorbents with low costs and high specific surface area [34,35].

This study aimed at modifying *L. minor* waste into activated carbon and investigates its potential in removing IPF from an aqueous solution. Governing operational

parameters examined include adsorbent mass, temperature, adsorption time, pH, and initial concentration. The experimental data were subjected isotherm model, that is, Langmuir, Freundlich, Temkin, and Dubinin–Radushkevich. Also, the kinetics of the adsorption process was correlated to four different models which include: pseudo-first-order, pseudo-second-order, film diffusion, and intraparticle diffusion models. Thermodynamic parameters were also calculated.

2. Materials and methods

2.1. Chemicals

IPF (98.0% purity) was purchased from Sigma Aldrich Co., Ltd., (USA). Its molecular structures and basic physicochemical parameters are provided in Table 1. All the other chemicals (analytical grade or better) were obtained from Merck Co., Ltd., (Germany), used with no further purification, and were diluted using ultrapure water (resistivity of 18.2 M Ω /cm at 25°C). The stock solutions (1,000 mg/L) of IPF were prepared in ultrapure water and stored in brown volumetric flasks at 25°C in the refrigerator before use. Working solutions of desired concentrations for each test were prepared by diluting the stock solution with ultrapure water.

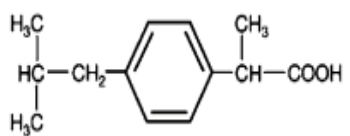
2.2. Point of zero charge pH

pH_{pzc} for the LMAC was determined by put of 0.12 g of LMAC in eight of 100 mL Erlenmeyer flasks which include 0.1 M NaNO_3 solution. The pH of the solutions was adjusted to 3, 4, 5, 6, 7, 8, 9, 10, and 11 with 0.01 or 0.1 mol/L HCL and NaOH. The solutions were equilibrated in an isothermal shaker (25°C) for 24 h. After the equilibrium, the final pH was determined. The pH_{pzc} means when the initial and final pHs are equal.

2.3. Preparation and characterization of the adsorbent

L. minor (LM), a kind of marine algae, was collected from the Anzali wetland, Iran, and used as activated carbon material. The collected LM was dried for 7 d after it was washed with deionized water. The dried LM was ground and manually sieved by 0.45 mm size screens. 100 g of the dried LM was immersed in 1 L of 28% zinc chloride (ZnCl_2) solution for 12 h, and then dried in an oven for 24 h at 105°C. The LM treated with ZnCl_2 solution was

Table 1
Ibuprofen molecular structure and physical chemical properties

CAS number	Molecular structure	Molecular weight	Molecular formula	pKa	Water solubility
15687-27-1		206.3 g/mol	$\text{C}_{16}\text{H}_{19}\text{N}_3\text{O}_5\text{S}$	4.91	210 mg/L

put in a sealed ceramic oven, and pyrolysis was applied to the LM under N_2 atmosphere at $350^\circ C$ for 2 h. The temperature of the oven was continuously raised to $650^\circ C$. The excess $ZnCl_2$ was removed from the resulting LMAC with hot 0.5 M HCl, and the LMAC was filtered and rinsed with warm water. Finally, the LMAC was dried was dried at $105^\circ C$ for 24 h [32]. The characteristics of the LMAC and IPF-loaded samples were expressed as surface morphology using an S-4800F field emission scanning electron microscopy (SEM, HITACHI). Determination of the surface area, total pore volume, and pore distribution of LMAC was conducted with N_2 adsorption ($-196^\circ C$) using a TRISTAR-3000 surface area and porosity analyzer (Micromeritics). The yield of prepared LMAC was calculated based on the following equation [33]:

$$Y (\%) = \frac{W_c}{W} \times 100 \quad (1)$$

where W_c and W are the weights of carbon product, and dried pods.

2.4. Adsorption studies

Adsorption was performed by the batch technique at $10^\circ C$, $25^\circ C$, $40^\circ C$, and $55^\circ C$ temperatures. The experiments were carried out in a series of 200 mL graduated conical flask containing 100 mL of solution of each concentration and a fixed amount of adsorbent. The initial pH of the solution was adjusted with 0.1 or 0.01 mol/L HCl and NaOH solutions by using a pH meter. Adsorption was achieved by adding a known amount of each adsorbent into the IPF solution of known concentration and pH, and the conical flask were agitated intermittently. The data obtained in the batch mode studies were used to calculate the equilibrium IPF adsorption amount at $25^\circ C \pm 2^\circ C$.

The residual amount of IPF in each flask was investigated using high-performance liquid chromatography (HPLC; C18 ODS column) with a UV detector 2006 at a wavelength of 230 nm. The 25 mM KH_2PO_4 at pH 3 (40%) and acetonitrile (60%) were used as the mobile phase and were delivered at 1 mL/min. A sample injection volume of 100 μL was used. The column temperature was maintained at $30^\circ C$. All experiments were conducted three times and the average values were shown. The amount of IPF adsorbed per unit adsorbent (mg IPF per g LMAC) and % removal was calculated according to a mass balance on the IPF concentration using Eqs. (2) and (3) [36,37]:

$$q_e = \frac{(C_0 - C_e)V}{M} \quad (2)$$

$$\text{Removal} (\%) = \frac{C_0 - C_e}{C_0} \times 100 \quad (3)$$

where V (L) is the IPF solution volume, C_0 is the initial concentration of IPF in mg/L, C_e (mg/L) is the liquid-phase concentration of IPF at time t (min), and M (g) is the weight of the LMAC.

3. Results and discussion

3.1. LMAC characterization

The characteristics of LMAC are summarized in Table 2. It is clearly seen from Table 2 that the LMAC had a specific surface area of $1,164.5 \text{ m}^2/\text{g}$, total pore volume of $0.417 \text{ cm}^3/\text{g}$, a porosity of 56.5%, and bulk density of $0.695 \text{ g}/\text{cm}^3$. The images of SEM of LMAC before and after adsorption are indicated in Fig. 1. The pores of the adsorbent were filled with IPF molecules after adsorption.

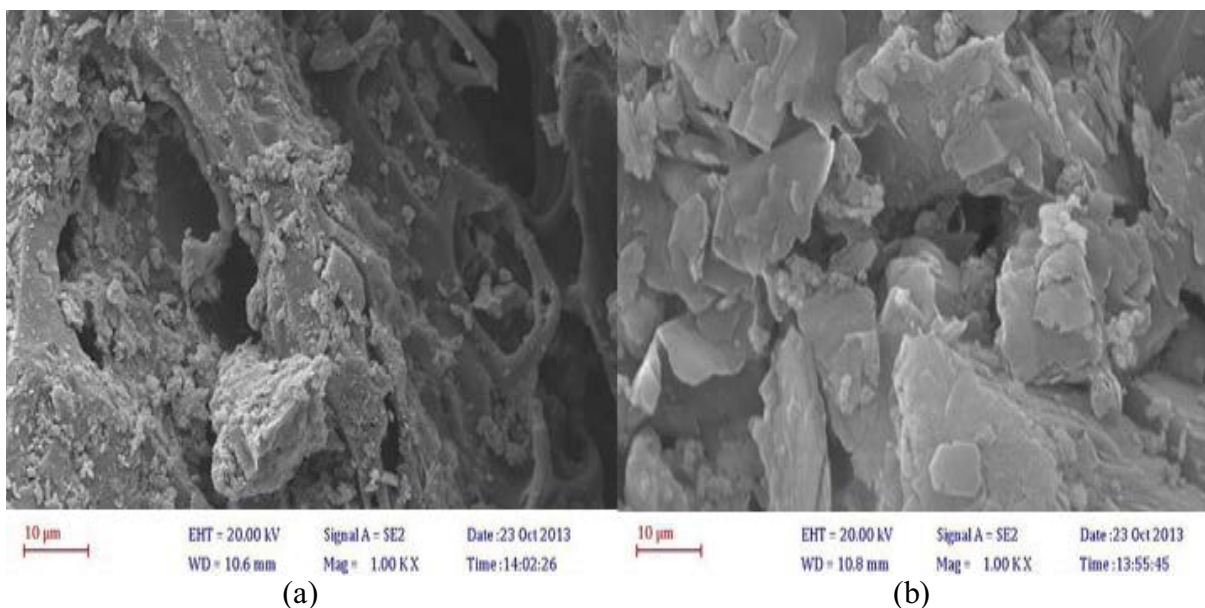


Fig. 1. SEM image of the LMAC adsorbent before (a) and after (b) adsorption.

Table 2
Important properties of the LMAC

Specific surface area	Average pore diameter	Porosity	Pore volume	Moisture	Bulk density
1,164.5 m ² /g	27.5 nm	56.5%	0.417 cm ³ /g	2.64%	0.695 g/cm ³
%Ash	C%	H%	N%	O%	Y
2.64	52.6	3.95	0.524	39.84	48.2%

Characteristics of the starting materials affected carbon texture and the development of porosity (Fig. 1). Fig. 2 illustrates the N₂ adsorption and pore size distribution of LMAC, indicating a type IV isotherm was revealed by the hysteresis loop at high P/P_0 values.

3.2. Effect of contact time and concentration on IPF adsorption

Fig. 3 shows the removal rate of IPF from an aqueous solution after contact with the LMAC (1.2 g) for various adsorption times. The removal rate was 91.5% after the initial 75 min of the contact time, indicating that a large number of adsorption sites were available on the adsorbent surface at the beginning of the adsorption process [38,39]. Thus, IPF molecules occupied these sites and were removed quickly from the aqueous solution. The remaining 8.5% of the IPF had a lower chance to interact with the adsorbent surface because the available adsorption sites were already occupied in the first 75 min of contact time [34]. Therefore, the adsorption of the remaining 8.5% of IPF molecules could only occur when the sites became available after desorption of a previously adsorbed molecule. This desorption occurs during the collision of fragments of molecules with other molecules [40]. Thus, the adsorption rate slowed and the removal of the remaining 8.5% of IPF required a longer contact time.

The effects of initial concentration IPF on the percentage of removal of IPF using LMAC were investigated within the concentration IPF range between 25 and 100 mg/L (Fig. 3). The IPF removal decreased with raising the initial concentration. This may be due to the limitation of free places available on LMAC for IPF adsorption. This finding is supported by the study carried out by Ghauch, who reported that the amoxicillin removal efficiencies decreased with the increasing initial concentration [38]. This observation also agreements with Ahmadi et al. [39].

3.3. Effect of LMAC mass on IPF adsorption

Fig. 4 displays the removal efficiency of IPF molecules from a 50 mg/L aqueous solution after a 75 min contact time with different doses of LMAC, increasing from 0.2 to 2 g in steps of 0.2 mg. It can be seen that, when the dose of LMAC was increased up to 1.2 g, the removal of IPF increased linearly. However, the addition of LMAC beyond 1.2 g did not increase the removal of IPF any further, indicating that the solution had reached a saturation point. Thus, it was concluded that 1.2 g was the optimal dose for the adsorbent to maximize the removal of IPF from the aqueous solution. The high IPF removal rate at this adsorbent dosage may be due to the greater number of adsorption sites on the

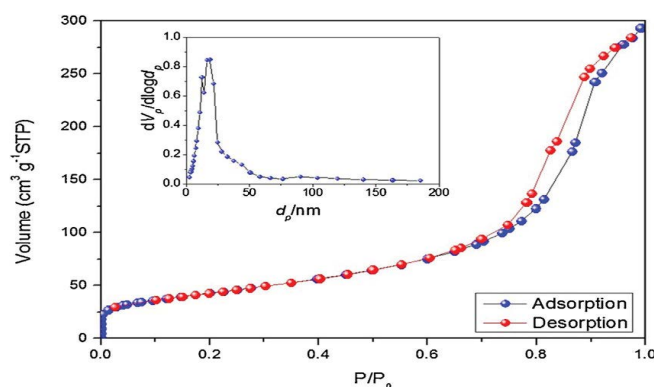


Fig. 2. N₂ adsorption and pore size distribution of LMAC.

surface of the adsorbent compared to the other doses [41]. This optimal dose was used for the subsequent experiments.

3.4. Determination of the pH_{pzc} and influence of solution pH

In this study, pH_{pzc} of the LMAC was used to estimate the effect of pH on the IPF removal rate. The pH_{pzc} of the pine cones LMAC was determined 6.6 (Fig. 5a). Changes in pH affected the dissociation of the IPF molecule. According to the dissociation constant of IPF ($pK_a = 4.91$), the anionic form of IPF predominates if adsorption occurs above pH 9. In addition, the solution pH values higher than 6.6 ($pH > pH_{pzc}$), overall surface charge on the LMAC is negative. In this case, electrostatic repulsion results in a reduction of adsorption capacity between the deprotonated IPF and the negatively charged activated carbon surface [41,42]. In contrast, the net charge on LMAC surface is positive in acidic solutions and IPF is mainly non-dissociated. Thus, minimal repulsive electrostatic interactions are observed and adsorption is strengthened (Fig. 5b). At pH above pH_{pzc} point, enhanced electrostatic repulsion between negatively charged IPF and the LMAC surfaces is responsible for the dramatic reduction in IPF adsorption [43]. Thus, as expected, IPF adsorption capacities of LMAC decreased when solution pH increased from strongly acidic to weakly alkaline conditions.

3.5. Adsorption kinetics

To investigate the influence of contact time, equilibrium adsorption studies were carried out for a pre-determined time interval (between 0 and 120 min), as shown in Fig. 6. Other operating conditions are as follows: pH of IPF was

the 5, initial IPF concentrations 25–100 mg/L, LMAC dose 1.2 g/L, temperature 25°C. The kinetic models can provide valuable information about the reaction pathways (adsorption rate and adsorbent/adsorbate interaction–physorption

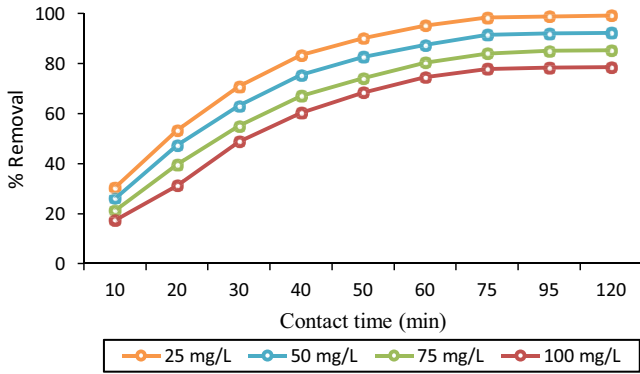


Fig. 3. Effect of contact time and concentration on IPF removal efficiency (LMAC mass = 1.2 g/L; pH = 5; temperature = 25°C).

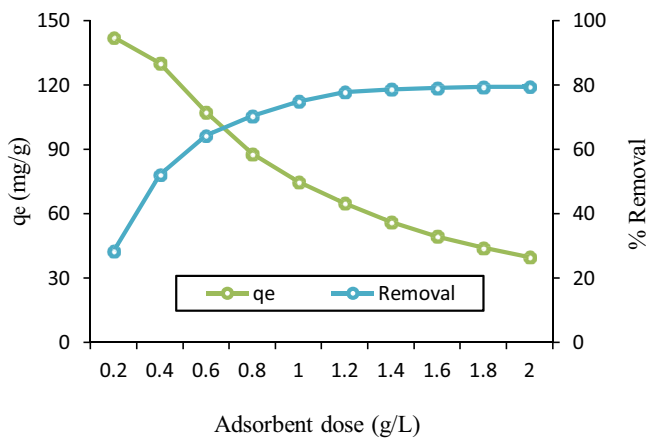


Fig. 4. Effect of LMAC mass on IPF removal efficiency ($C_0 = 100$ mg/L; pH = 5; time = 75 min; temperature = 25°C).

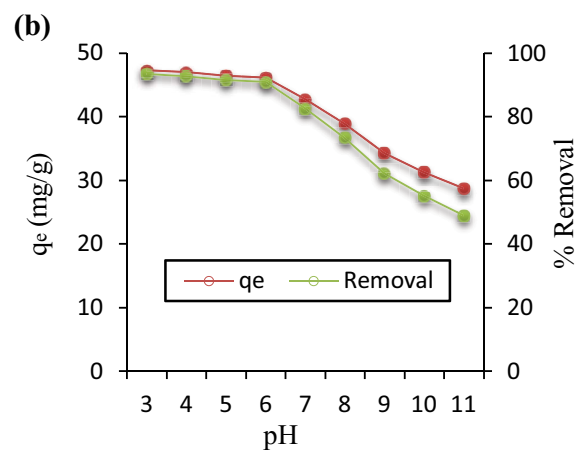
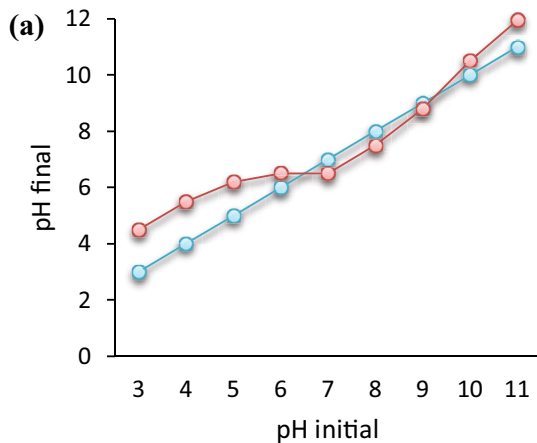


Fig. 5. (a) Determination of the point of zero charge of LMAC and (b) effect of solution pH on the removal percentage of IPF ($C_0 = 50$ mg/L; LMAC mass = 1.2 g/L; time = 75 min; temperature = 25°C).

or chemisorption). In this context, pseudo-first-order model and pseudo-second-order model were used to analyze the kinetic adsorption data. In addition, possible adsorption mechanisms were evaluated by intra-particle diffusion and film diffusion. Kinetics parameters were calculated using the following equations [44–47]:

Pseudo-first-order model:

$$\ln(q_e - q_t) = \ln q_e - K_1 t \quad (4)$$

Pseudo-second-order model:

$$\frac{t}{q_t} = \frac{1}{K_2 q_e^2} + \frac{t}{q_e} \quad (5)$$

Film diffusion model:

$$\ln\left(1 - \frac{q_t}{q_e}\right) = -K_3 t + C \quad (6)$$

Intra-particle diffusion model:

$$q_t = K_b t^{1/2} + I \quad (7)$$

where q_e (mg/g) q_t and (mg/g) are the amounts of IPF adsorbed on the LMAC at equilibrium and at time t (min), respectively, K_1 (1/min) is the rate constant of pseudo-first-order adsorption. K_2 (g/mg min) is the rate constant of pseudo-second-order adsorption. K_3 (1/min) and I are liquid film diffusion constants, K_b where (mg/g min^{0.5}) is the rate constant of intra-particle diffusion model, and I (mg/g) is a constant describing the thickness of boundary layer.

The kinetic parameters, q_e , q_t , K_1 , and K_2 were calculated based Eqs. (4) and (5) and are presented in Figs. 6a and b and Table 3, respectively. The calculated adsorption capacity ($q_{e,cal}$) based on the pseudo-first-order kinetic model differed considerably from the experimental adsorption capacity ($q_{e,exp}$). In contrast, the $q_{e,cal}$ determined using the pseudo-second-order kinetic model was similar to $q_{e,exp}$. Fig. 6b also shows that a closer linear fit was obtained

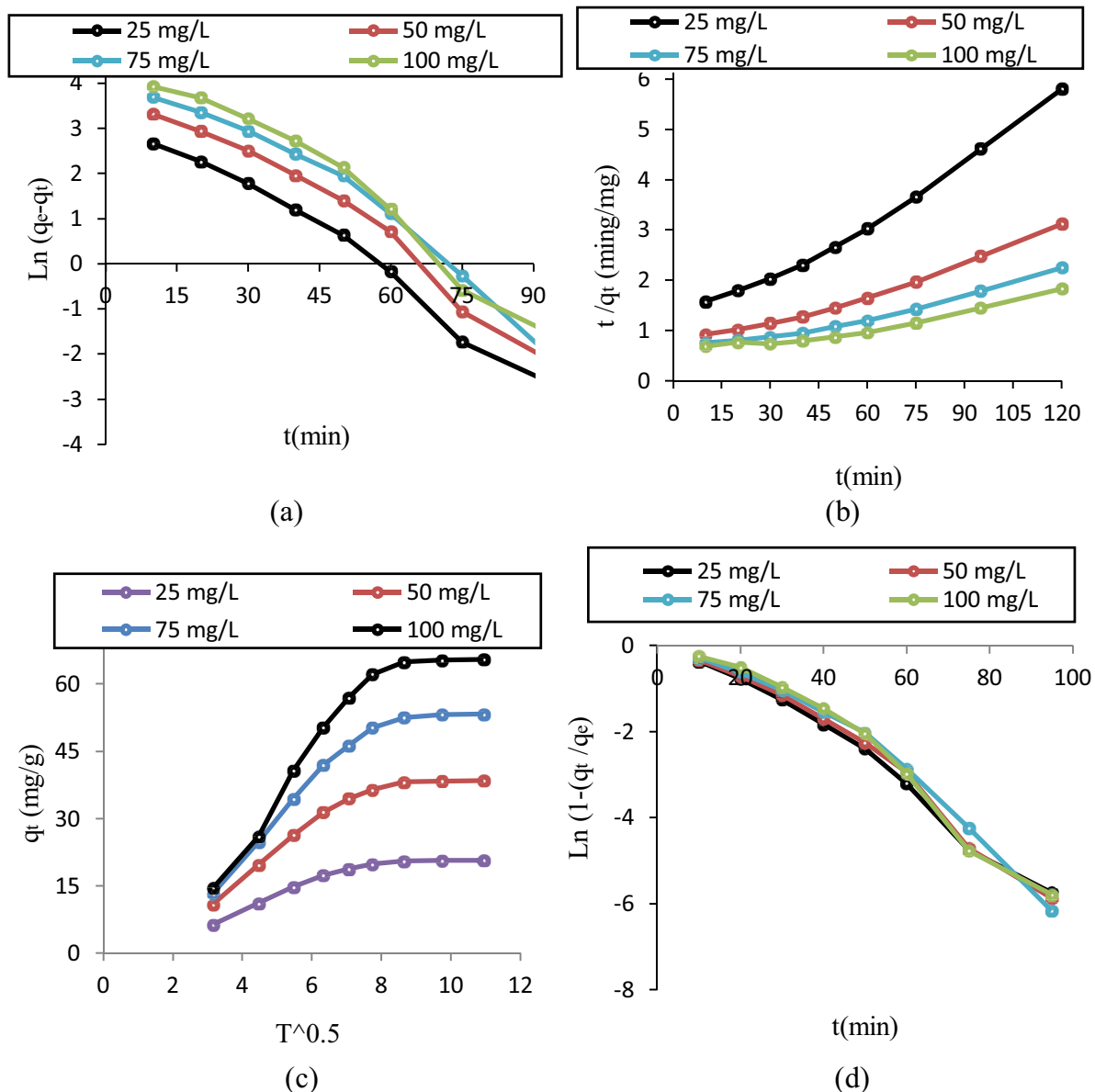


Fig. 6. Linear fit of the adsorption kinetics for IPF removal by LMAC: (a) pseudo-first-order, (b) pseudo-second-order, (c) intra-particle diffusion, and (d) film diffusion kinetic models.

using pseudo-second-order reaction kinetics compared to pseudo-first-order reaction kinetics (Fig. 6a). Thus, based on these results, LMAC clearly followed pseudo-second-order reaction kinetics in the removal of IPF from an aqueous solution. As a result, chemisorption might have been the major adsorption mechanism, electron donor-acceptor, and π - π dispersion interaction may act simultaneously in the adsorption of adsorbate on LMAC [48,49].

Adsorption kinetics is usually controlled simultaneously by film diffusion and intra-particle diffusion. The adsorption behavior of the IPF/LMAC system can be further explored using the above two diffusion models to determine the type of rate-controlling step. Figs. 6c and d show the plots obtained for film diffusion and intra-particle diffusion models, and the related parameters are listed in Table 3.

The adsorption of IPF on LMAC mainly exhibited two stages (stages I and II), which was related to the changes in mass transfer rates during the adsorption process. Stage I represents the rapid adsorption (film diffusion), which was attributed to the diffusion of IPF through the liquid film surrounding the surface of the LMAC. Although the plots present some linearity ($R^2 > 0.96$), the slope did not cross the origin, attesting the involvement of film diffusion in the adsorption reaction process [50]. Stage II was a more gradual adsorption (intra-particle diffusion), corresponding to the IPF transport within the inner LMAC surface, which was attributed to the higher internal diffusion ability at the initial adsorbate concentration [51]. However, the plots did not pass through the origin, which was indicative of boundary layer presence, attesting the intra-particle diffusion

Table 3
Results of kinetic model studies related to the IPF adsorption onto LMAC

C ₀ (mg/L)	q _{e,exp} (mg/g)	Intra diffusion		Film diffusion		Pseudo-first order			Pseudo-second order		
		K _b	R ²	K ₃	R ²	q _{e,cal}	K ₁	R ²	q _{e,cal}	K ₂	R ²
25	20.67	1.82	0.824	0.066	0.982	11.95	0.066	0.962	26.31	0.0016	0.992
50	38.47	3.55	0.842	0.067	0.972	18.74	0.067	0.972	39.21	0.00118	0.989
75	53.30	5.27	0.861	0.068	0.962	26.19	0.068	0.962	52.63	0.0007	0.995
100	65.48	6.92	0.858	0.071	0.965	35.52	0.069	0.965	66.66	0.0004	0.991

mechanism was not the rate-determining step. Hence, both of these mechanisms were possible.

3.6. Adsorption isotherm

To gain further insights into the adsorption mechanism of IPF onto LMAC, four widely used Langmuir, Freundlich, Temkin, and D–R models were adopted for fitting the adsorption equilibrium data. The linear forms of the Langmuir, Freundlich, Temkin, and D–R isotherms are represented by the following equations [52–54]:

Langmuir:

$$\frac{1}{q_e} = \frac{1}{q_m} + \frac{1}{K_L C_e q_m} \tag{8}$$

Freundlich:

$$\log q_e = \frac{1}{n} \log C_e + \log K_f \tag{9}$$

Temkin:

$$q_e = \frac{RT}{\beta_T} \ln(K_T C_e) \tag{10}$$

D–R:

$$\ln q_e = \ln q_m - \left(\frac{RT}{\sqrt{2E}} \right)^2 \times \left(\ln \left(1 + \frac{1}{C_e} \right) \right)^2 \tag{11}$$

where q_m (mg/g) is the Langmuir maximum adsorption capacity of IPF, K_L (L/mg) is the Langmuir constant termed as apparent energy of adsorption, K_f ((mg/g) (L/mg)^{1/n}) is the Freundlich constants related to adsorption capacity, n is a measure of adsorption linearity, β_T (J/mol) is the Temkin constant related to the heat of adsorption, K_T (L/g) is the Temkin isotherm constant, R (8.314 J/mol K) is the gas constant, T (K) is the absolute temperature, q_m (mg/g) is the D–R maximum adsorption capacity of IPF, and E (J/mol) is mean free energy of adsorption per molecule of the adsorbate.

The isotherm constants for adsorption of IPF onto LMAC at different temperatures are shown in Table 4. The detailed analysis of the correlation coefficient R² values showed that the Langmuir model (0.991–0.995) fit the experiments data better than the other models at different temperatures (Fig. 7). From Table 4, it is also clear that the q_m (Langmuir and D–R) increased when the temperature

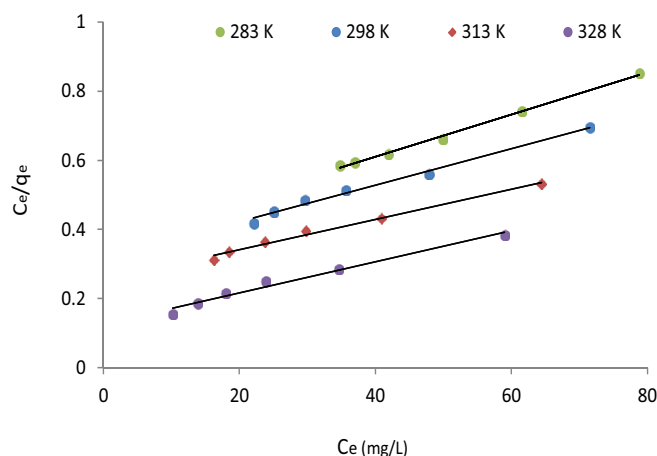


Fig. 7. Langmuir isotherm models for the adsorption of IPF by LMAC.

Table 4
Isotherm parameters for adsorption of IPF onto LMAC at various temperatures

Isotherm models	283 K	298 K	313 K	328 K
Langmuir				
q _m (mg/g)	124.5	141.8	159.2	181.2
K _L (L/mg)	0.0019	0.0028	0.0059	0.0078
R _L	0.841	0.781	0.628	0.561
R ²	0.991	0.995	0.992	0.994
Freundlich				
K _F	3.478	5.149	6.496	8.137
1/n	0.774	0.593	0.448	0.389
R ²	0.901	0.923	0.913	0.908
Temkin				
K _T	1.559	2.176	1.925	3.814
B _T	95.87	91.14	81.03	69.58
R ²	0.845	0.838	0.865	0.869
D–R				
q _m (mg/g)	161.2	176.8	189.9	201.4
E	1.325	1.843	2.176	2.395
R ²	0.943	0.948	0.951	0.961

increased, once again indicating the adsorption was an endothermic process [55]. Also, the Langmuir constant (K_L) increased with increasing temperature, indicating that the adsorption process was endothermic [56].

The maximum adsorption capacity of IPF onto LMAC was 124.5, 141.8, 159.2, and 181.2 mg/g at 283, 298, 313, and 328 K, respectively. Also, the comparison of adsorption capacities for the removal of antibiotics from aqueous solution using different adsorbent is represented in Table 5. It was subsequently found that the removal of IPF onto LMAC was better than the other adsorbents, meaning that our proposed LMAC are more suitable for use in environmental remediation, particularly because carbonization is a simple process. Also, carbonization increases the total number of adsorption sites on the *L. minor*, thus enhancing the adsorption of IPF.

The essential features of the Langmuir isotherm are expressed by a dimensionless constant separation factor R_L , it can be expressed as follows [57]:

$$R_L = \frac{1}{1 + K_L C_0} \quad (12)$$

where C_0 is the IPF initial concentration (mg/L). The value of R_L indicates the shape of isotherm to be either irreversible ($R_L = 0$) or favorable ($0 < R_L < 1$) or linear ($R_L = 1$) or unfavorable ($R_L > 1$). The results showed that the R_L values (listed in Table 4) were all in the range of 0–1 at 283°C–328°C, indicating that the LMAC is favorable for adsorption of IPF under the studied conditions. There is increase in the K_F value at 328 K compare to that of 283 K. This suggests a higher affinity for the adsorbate at higher temperatures [58,59]. The low E -value (< 8 kJ/mol) in D–R at different temperatures confirms the adsorption process to be physical [38]. The highest R^2 value seen with the Langmuir isotherm model suggests this model as an appropriate model capable of explaining the adsorption of IPF onto LMAC.

3.7. Effect of temperature and determination of thermodynamic parameters

The adsorption of IPF was studied at different temperatures using LMAC as an adsorbent (Fig. 8). The experimental result shows that the removal of IPF increased with increase in the solution temperature from 283–328 K.

Table 5
Maximum adsorption capacities (q_{\max}) of some adsorbents for different antibiotics

Adsorbent	Antibiotic	q_{\max} (mg/g)	References
Magnetic graphene oxide	Amoxicillin	112.6	[45]
Organobentonite	Amoxicillin	30.12	[48]
Activated carbon	Ibuprofen	96.44	[7]
Bentonite	Amoxicillin	47.37	[32]
Powder activated carbon magnetized by Fe_3O_4 nanoparticles	Amoxicillin	116.98	[49]
CdS-MWCNT nanocomposites	Cefotaxime	40.525	[50]
	Cefradine	37.714	
	Cefazolin	34.215	
Walnut shell-based activated carbon	Cephalexin	141.1	[51]
	MgO nanoparticles	Cephalexin	48.24
BSA/ Fe_3O_4 magnetic composite microspheres	Cefixime	93.1	[53]
	Streptomycin	69.35	
	Tetracycline	104.25	
	Chloramphenicol	117.83	
Magnetically modified graphene nanoplatelets	Erythromycin	114.51	[54]
	Amoxicillin	14.10	
	Microporous activated carbon	Ciprofloxacin	
Activated carbon	Norfloxacin	116.99	[56]
	Trimethoprim	57.92	
<i>Azolla filiculoides</i>	Penicillin G	4.12	[40]
Olive waste cakes	Ibuprofen	12.6	[57]
Potato peels	Dorzolamide	52.1	[58]
Cattail fiber	Acetaminophen	59.9	[59]
Lotus stalks	Cephalexin	66.2	[60]
LMAC	Ibuprofen	Temperature 283 K = 124.5	This study
		Temperature 298 K = 141.8	
		Temperature 313 K = 159.2	
		Temperature 328 K = 181.2	

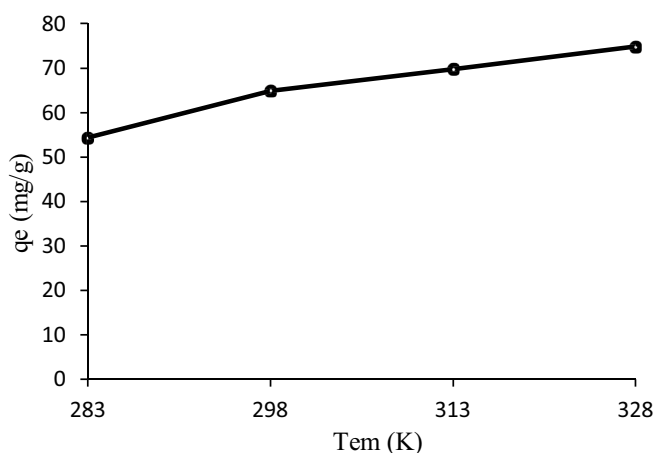


Fig. 8. Effect of temperature on adsorption capacity ($C_0 = 100$ mg/L; pH = 5; time = 75 min; LMAC mass = 1.2 g/L).

This indicates that the adsorption of IPF onto LMAC is endothermic in nature.

The adsorption nature of adsorption systems was further demonstrated by evaluation of changes in Gibbs free energy (ΔG°), enthalpy (ΔH°), and entropy (ΔS°). The amount of ΔG° , ΔH° , and ΔS° were calculated as follows [60–62]:

$$\Delta G^\circ = -RT \ln K_b \quad (13)$$

$$\Delta G^\circ = \Delta H^\circ - T\Delta S^\circ \quad (14)$$

$$\ln K_b = \frac{\Delta S^\circ}{R} - \frac{\Delta H^\circ}{RT} \quad (15)$$

where $K_b = q_e/C_e$ is the equilibrium constant, which q_e is the concentration of the solid phase at equilibrium (mg/g), and C_e is the concentration at equilibrium (mg/L), R is the constant of the ideal gases 8,314 J/mol K, T is the absolute temperature at K. The (ΔH°) and (ΔS°) are determined from the slope and the y -axis intercept of $\ln K_b$ vs. $1/T$. The calculated values of the three parameters are shown in Table 6. The negative values of Gibbs free energy indicated that the adsorption of IPF was thermodynamically spontaneous and favorable [63]. The more negative values with increasing temperature implied stronger adsorption driving force at higher temperature [64]. Moreover, all computed were within the range of -20 to 0 KJ/mol, confirming the physical nature of the adsorption, which

shows consistency with the conclusion obtained from D–R isotherm analysis [65]. The obtained positive values of enthalpy, revealed the endothermic nature of IPF adsorption and high temperature favored the adsorption process [66]. Finally, the positive values of entropy reveal the affinity between the IPF and LMAC with an increase in degree of freedom [67]. It also shows increase in the randomness at adsorbate–solution interface during the adsorption process.

4. Conclusions

This is the first study on the adsorption of IPF by LMAC. The following conclusions could be summarized as follows: (1) the thermodynamic parameters of adsorption systems implied that the adsorption was endothermic and spontaneous under examined conditions. (2) In adsorption system, physisorption may occur during the adsorption process. The adsorption equilibrium data could be satisfactorily explained by Langmuir isotherm, indicating that the adsorption was monolayer adsorption. (3) Batch adsorption study was performed to analyze the effect of initial concentration, contact time, pH, temperature, and adsorbent dose on adsorption of IPF on LMAC. It was observed that maximum IPF adsorption was achieved at pH 3 at an optimum equilibrium contact time of 75 min and temperature 328 K with an adsorbent dose of 1.2 g/L and concentration 25 mg/L. (4) The pseudo-second-order kinetic described better the adsorption system based on a comparison of the kinetic models on the overall adsorption rate. (5) This study demonstrated that the LMAC could be used as an effective adsorbent for the treatment of wastewater containing IPF antibiotics.

Acknowledgments

We thank all those who have helped us conduct this study, especially the officials of the chemistry laboratory at the department of environmental health engineering and Zahedan University of Medical Sciences for the financial support of this study.

Author contributions

DB (professor) designed and controlled all this study, overall as the first author. ZT (researcher) conducted all the experiments and wrote the manuscript. MS (researcher) conducted all the analyses and revised the manuscript. S-ML (professor) revised the manuscript as a co-corresponding author. CJ (professor) revised and wrote the manuscript as a co-corresponding author.

Table 6
Values of thermodynamic parameters for the adsorption of IPF onto LMAC

Temperature (K)	ΔG° (kJ/mol)	ΔH° (kJ/mol)	ΔS° (kJ/mol K)
283	-1.01		
298	-2.58		
313	-3.67	25.12	0.092
328	-5.27		

References

- [1] T. Garoma, S.H. Umamaheshwar, A. Mumper, Removal of sulfadiazine, sulfamethizole, sulfamethoxazole, and sulfathiazole from aqueous solution by ozonation, *Chemosphere*, 79 (2010) 814–820.
- [2] R. Alexy, T. Kumpel, K. Kummerer, Assessment of degradation of 18 antibiotics in the closed bottle test, *Chemosphere*, 57 (2004) 505–512.
- [3] K.J. Choi, S.G. Kim, S.H. Kim, Removal of antibiotics by coagulation and granular activated carbon filtration, *J. Hazard. Mater.*, 151 (2008) 338–343.
- [4] D. Balarak, F.K. Mostafapour, Photocatalytic degradation of amoxicillin using UV/Synthesized NiO from pharmaceutical wastewater, *Indonesia J. Chem.*, 19 (2019) 211–218.
- [5] D. Balarak, F.K. Mostafapour, H. Azarpira, Adsorption isotherm studies of tetracycline antibiotics from aqueous solutions by maize stalks as a cheap biosorbent, *Int. J. Pharm. Technol.*, 8 (2016) 16664–16675.
- [6] D. Balarak, F.K. Mostafapour, E. Bazrafshan, T.A. Saleh, Studies on the adsorption of amoxicillin on multi-wall carbon nanotubes, *Water Sci. Technol.*, 75 (2017) 1599–1606.
- [7] S.K. Behera, S.Y. Oh, H.S. Park, Sorptive removal of ibuprofen from water using selected soil minerals and activated carbon, *Int. J. Environ. Sci. Technol.*, 9 (2012) 85–94.
- [8] L.H. Heckmann, A.C. Helen, L. Hooper, R. Connon, T.H. Hutchinson, S.J. Maund, R.M. Sibly, Chronic toxicity of ibuprofen to *Daphnia magna*: effects on life history traits and population dynamics, *Toxicol. Lett.*, 172 (2007) 137–145.
- [9] M. Melillo, V.M. Gun'ko, S.R. Tennison, L.I. Mikhailovska, G.J. Phillips, J.G. Davies, Structural characteristics of activated carbons and ibuprofen adsorption affected by Bovine serum albumin, *Langmuir*, 20 (2004) 2837–2851.
- [10] A.S. Mestre, J. Pires, J.M.F. Nogueira, A.P. Carvalho, Activated carbons for the adsorption of ibuprofen, *Carbon*, 45 (2007) 1979–1988.
- [11] A.S. Mestre, J. Pires, J.M.F. Nogueira, J.B. Parra, Waste-derived activated carbons for removal of ibuprofen from solution: role of surface chemistry and pore structure, *Bioresour. Technol.*, 100 (2007) 1720–1726.
- [12] R. Rostamian, H. Behnejad, A comparative adsorption study of sulfamethoxazole onto graphene and graphene oxide nanosheets through equilibrium, kinetic and thermodynamic modeling, *Proc. Saf. Environ. Prot.*, 102 (2016) 20–29.
- [13] A.H. Mahvi, F.K. Mostafapour, Biosorption of tetracycline from aqueous solution by *Azolla filiculoides*: equilibrium kinetic and thermodynamics studies, *Fresenius Environ. Bull.*, 27 (2018) 5759–5767.
- [14] X.D. Zhu, Y.J. Wang, R.J. Sun, D.M. Zhou, Photocatalytic degradation of tetracycline in aqueous solution by nanosized TiO₂, *Chemosphere*, 92 (2013) 925–932.
- [15] M.E. Parolo, M.C. Savini, J.M. Vallés, M.T. Baschini, M.J. Avena, Tetracycline adsorption on montmorillonite: pH and ionic strength effects, *Appl. Clay Sci.*, 40 (2008) 179–186.
- [16] D. Balarak, H. Azarpira, F.K. Mostafapour, Study of the adsorption mechanisms of cephalexin on to *Azolla filiculoides*, *Pharm. Chem.*, 8 (2016) 114–121.
- [17] L. Ji, W. Chen, L. Duan, D. Zhu, Mechanisms for strong adsorption of tetracycline to carbon nanotubes: a comparative study using activated carbon and graphite as adsorbents, *Environ. Sci. Technol.*, 43 (2009) 2322–2327.
- [18] L. Zhang, X. Song, X. Liu, L. Yang, F. Pan, Studies on the removal of tetracycline by multi-walled carbon nanotubes, *Chem. Eng. J.*, 178 (2011) 26–33.
- [19] M. Kamranifar, F. Safari, A. Naghizadeh, Mechanism, kinetics and thermodynamic of Penicillin G antibiotic removal by silica nanoparticles from simulated hospital wastewater, *Desal. Water Treat.*, 169 (2019) 333–341.
- [20] M. Kamranifar, A. Allahresani, A. Naghizadeh, Application of CoFe₂O₄@CuS magnetic nanocomposite as a novel adsorbent for removal of Penicillin G from aqueous solutions: isotherm, kinetic and thermodynamic study, *Desal. Water Treat.*, 148 (2019) 363–373.
- [21] M. Kamranifar, A. Allahresani, A. Naghizadeh, Synthesis and characterizations of a novel CoFe₂O₄@CuS magnetic nanocomposite and investigation of its efficiency for photocatalytic degradation of penicillin G antibiotic in simulated wastewater, *J. Hazard. Mater.*, 366 (2019) 545–555.
- [22] R. Kamaraj, S. Vasudevan, Decontamination of selenate from aqueous solution by oxidized multi-walled carbon nanotubes, *Powder Technol.*, 274 (2015) 268–275.
- [23] P. Ganesan, R. Kamaraj, G. Sozhan, S. Vasudevan, Oxidized multi-walled carbon nanotubes as adsorbent for the removal of manganese from aqueous solution, *Environ. Sci. Pollut. Res.*, 20 (2013) 987–996.
- [24] R. Kamaraj, P. Pandiarajan, G.A. Shibayama, S. Vasudevan, Eco-friendly and easily prepared graphene nanosheets for safe drinking water: removal of chloro-phenoxyacetic acid herbicides, *ChemistrySelect*, 2 (2017) 342–355.
- [25] A. Carabineiro, T. Thavorn-Amornsri, F. Pereira, L. Figueiredo, Adsorption of ciprofloxacin on surface modified carbon materials, *Water Res.*, 145 (2011) 4583–4591.
- [26] L. Huang, M. Wang, C. Shi, J. Huang, B. Zhang, Adsorption of tetracycline and ciprofloxacin on activated carbon prepared from lignin with H₃PO₄ activation, *Desal. Water Treat.*, 52 (2014) 2678–2687.
- [27] J.A. Muthanna, M.J. Ahmed, S.K. Theydan, Adsorption of cephalexin onto activated carbons from *Albizia lebbek* seed pods by microwave-induced KOH and K₂CO₃ activations, *Chem. Eng. J.*, 211 (2012) 200–207.
- [28] R.A. Diyanati, Z. Yousefi, J.Y. Cherati, The ability of *Azolla* and *Lemna minor* biomass for adsorption of phenol from aqueous solutions, *J. Mazandaran Univ. Med. Sci.*, 23 (2013) 17–23.
- [29] R.A. Diyanati, J. Yazdani, Effect of sorbitol on phenol removal rate by *Lemna minor*, *J. Mazandaran Univ. Med. Sci.*, 22 (2013) 58–64.
- [30] Y. Uysal, Removal of chromium ions from wastewater by duckweed, *Lemna minor* L. by using a pilot system with continuous flow Y, *J. Hazard. Mater.*, 263 (2013) 486–492.
- [31] D. Balarak, F.K. Mostafapour, H. Azarpira, Adsorption kinetics and equilibrium of ciprofloxacin from aqueous solutions using corylusavellana (hazelnut) activated carbon, *Br. J. Pharm. Res.*, 13 (2016) 1–14.
- [32] E.K. Putra, R. Pranowoa, J. Sunarsob, N. Indraswatia, S. Ismadjia, Performance of activated carbon and bentonite for adsorption of amoxicillin from wastewater: mechanisms, isotherms and kinetics, *Water Res.*, 43 (2009) 2419–2430.
- [33] X. Peng, F. Hu, H. Dai, Q. Xiong, Study of the adsorption mechanism of ciprofloxacin antibiotics onto graphitic ordered mesoporous carbons, *J. Taiwan Inst. Chem. Eng.*, 8 (2016) 1–10.
- [34] Y. Gao, Y. Li, L. Zhang, H. Huang, J. Hu, Adsorption and removal of tetracycline antibiotics from aqueous solution by graphene oxide, *J. Colloid Interface Sci.*, 368 (2012) 540–546.
- [35] Z. Liu, H. Xie, J. Zhang, C. Zhang, Sorption removal of cephalexin by HNO₃ and H₂O₂ oxidized activated carbons, *Sci. China Chem.*, 55 (2012) 1959–1967.
- [36] M. Jafari, S.F. Aghamiri, G. Khaghanic, Batch adsorption of cephalosporins antibiotics from aqueous solution by means of multi-walled carbon nanotubes, *World Appl. Sci. J.*, 14 (2011) 1642–1650.
- [37] R. Al-Khalisy, A. Al-Haidary, A. Al-Dujaili, Aqueous phase adsorption of cephalexin onto Bentonite and activated carbon, *Sep. Sci. Technol.*, 45 (2010) 1286–1294.
- [38] A. Ghauch, A. Tuqan, H.A. Assi, Elimination of amoxicillin and ampicillin by micro scale and nano scale iron particles, *Environ. Pollut.*, 157 (2009) 1626–1635.
- [39] S. Ahmadi, A. Banach, F.K. Mostafapour, Study survey of cupric oxide nanoparticles in removal efficiency of ciprofloxacin antibiotic from aqueous solution: adsorption isotherm study, *Desal. Water Treat.*, 89 (2017) 297–303.
- [40] M. Malakootian, Y. Mahdavi, S.H. Sadeghi, N. Amirmahani, Removal of antibiotics from wastewater by *Azolla filiculoides*: kinetic and equilibrium studies, *Int. J. Anal. Pharm. Biomed. Sci.*, 4 (2015) 105–113.

- [41] H. Azarpira, Y. Mahdavi, O. Khaleghi, Thermodynamic studies on the removal of metronidazole antibiotic by multi-walled carbon nanotubes, *Pharm. Lett.*, 8 (2016) 107–113.
- [42] W. Chih-Jen, L. Zhaohui, J. Wei-Teh, Adsorption of ciprofloxacin on 2:1 dioctahedral clay minerals, *Appl. Clay Sci.*, 53 (2011) 723–728.
- [43] M. Erşan, E. Bağd, Investigation of kinetic and thermodynamic characteristics of removal of tetracycline with sponge like, tannin based cryogels, *Colloids Surf., B*, 104 (2013) 75–82.
- [44] D. Balarak, H. Azarpira, Rice husk as a biosorbent for antibiotic metronidazole removal: isotherm studies and model validation, *Int. J. ChemTech. Res.*, 9 (2016) 566–573.
- [45] S.E. Moradi, Highly efficient removal of amoxicillin from water by magnetic graphene oxide adsorbent, *Chem. Bull. Politehnica Univ. Timisoara*, 60 (2015) 41–48.
- [46] S. Vasudevan, J. Lakshmi, The adsorption of phosphate by graphene from aqueous solution, *RSC Adv.*, 2 (2012) 5234–5242.
- [47] S. Vasudevan, J. Lakshmi, G. Sozhan, Studies relating to removal of arsenate by electrochemical coagulation: optimization, kinetics, coagulant characterization, *Sep. Sci. Technol.*, 45 (2010) 1313–1325.
- [48] S.X. Zha, Y. Zhou, X. Jin, Z. Chen, The removal of amoxicillin from wastewater using organobentonite, *J. Environ. Manage.*, 129 (2013) 569–576.
- [49] B. Kakavandi, R. Kalantary, A. Jonidi Jafari, A. Esrafily, A. Gholizadeh, A. Azari, Efficiency of powder activated carbon magnetized by Fe_3O_4 nanoparticles for amoxicillin removal from aqueous solutions: equilibrium and kinetic studies of adsorption process, *Iran. J. Health Environ.*, 7 (2014) 21–34.
- [50] A. Fakhri, S. Rashidi, M. Asif, I. Tyagi, S. Agarwal, V.K. Gupta, Dynamic adsorption behavior and mechanism of cefotaxime, cefradine and cefazolin antibiotics on CdS-MWCNT nanocomposites, *J. Mol. Liq.*, 215 (2016) 269–275.
- [51] G. Nazari, H. Abolghasemi, M. Esmaili, Batch adsorption of cephalixin antibiotic from aqueous solution by walnut shell-based activated carbon, *J. Taiwan Inst. Chem. Eng.*, 58 (2016) 357–365.
- [52] A. Fakhri, S. Adami, Adsorption and thermodynamic study of Cephalosporins antibiotics from aqueous solution onto MgO nanoparticles, *J. Taiwan Inst. Chem. Eng.*, 45 (2014) 1001–1006.
- [53] B. Zhang, H. Zhang, X. Li, X. Lei, C. Li, D. Yin, Synthesis of BSA/ Fe_3O_4 magnetic composite microspheres for adsorption of antibiotics, *Mater. Sci. Eng.*, 33 (2013) 4401–4408.
- [54] O. Kerkez-Kuyumcu, S.S. Bayazit, M.A. Salam, Antibiotic amoxicillin removal from aqueous solution using magnetically modified graphene nanoplatelets, *J. Ind. Eng. Chem.*, 35 (2016) 225–234.
- [55] M.J. Ahmed, S.K. Theydan, Fluoroquinolones antibiotics adsorption onto microporous activated carbon from ligno-cellulosic biomass by microwave pyrolysis, *J. Taiwan Inst. Chem. Eng.*, 45 (2014) 219–226.
- [56] H. Azarpira, Y. Mahdavi, Removal of Cd(II) by adsorption on agricultural waste biomass, *Pharm. Chem.*, 8 (2016) 61–67.
- [57] S.H. Kim, H.K. Shon, H.H. Ngo, Adsorption characteristics of antibiotics trimethoprim on powdered and granular activated carbon, *J. Ind. Eng. Chem.*, 16 (2010) 344–349.
- [58] R. Baccar, M. Sarrà, J. Bouzid, M. Feki, P. Blázquez, Removal of pharmaceutical compounds by activated carbon prepared from agricultural by-product, *Chem. Eng. J.*, 211 (2012) 310–317.
- [59] G.Z. Kyzas, E.A. Deliyanni, Modified activated carbons from potato peels as green environmental-friendly adsorbents for the treatment of pharmaceutical effluents, *Chem. Eng. Res. Des.*, 25 (2014) 19–26.
- [60] L. Hai, W. Ning, P. Cheng, J. Zhang, Y. Wang, Evaluation of animal hairs-based activated carbon for sorption of norfloxacin and acetaminophen by comparing with cattail fiber-based activated carbon, *J. Anal. Appl. Pyrolysis*, 101 (2013) 156–165.
- [61] H. Liu, W. Liu, J. Zhang, C. Zhang, L. Ren, Y. Li, Removal of cephalixin from aqueous solution by original and Cu(II)/Fe(III) impregnated activated carbons developed from lotus stalks kinetics and equilibrium studies, *J. Hazard. Mater.*, 185 (2011) 1528–1535.
- [62] L. Xu, J. Pan, J. Dai, X. Li, H. Hang, Z. Cao, Y. Yan, Preparation of thermal-responsive magnetic molecularly imprinted polymers for selective removal of antibiotics from aqueous solution, *J. Hazard. Mater.*, 233–234 (2012) 48–56.
- [63] S. Vasudevan, J. Lakshmi, G. Sozhan, Optimization of the process parameters for the removal of phosphate from drinking water by electrocoagulation, *Desal. Water Treat.*, 12 (2009) 407–414.
- [64] J.W. Peterson, L.J. Petrasky, M.D. Seymour, Adsorption and breakdown of penicillin antibiotic in the presence of titanium oxide nanoparticles in water, *Chemosphere*, 87 (2012) 911–917.
- [65] F. Yu, Y. Li, S. Han, M. Jie, Adsorptive removal of antibiotics from aqueous solution using carbon materials, *Chemosphere*, 153 (2016) 365–385.
- [66] S. Vasudevan, J. Lakshmi, Electrochemical removal of boron from water: adsorption and thermodynamic studies, *Can. J. Chem. Eng.*, 90 (2012) 1017–1026.
- [67] D. Balarak, F.K. Mostafapour, A. Joghataei, Adsorption of Acid Blue 225 dye by multi walled carbon nanotubes: determination of equilibrium and kinetics parameters, *Pharm. Chem.*, 8 (2016) 138–145.